Geomagnetic and Telluric Field Variability as a Driver of Geomagnetically Induced Currents

O. Kozyreva, V. Pilipenko, E. Sokolova, Ya. Sakharov and D. Epishkin

Abstract We analyse temporal and spatial variability of geomagnetic and telluric electric fields in the Eastern Fennoscandia. These variations are compared with available geomagnetically induced current (GICs) measurements in electric power transmission lines at Kola Peninsula and Karelia. The information on impedance tensors is provided by the electromagnetic sounding array BEAR. We synthesize the telluric E-field from geomagnetic field variations, using the complex impedance tensor. We analyze geomagnetic and E-field variations at several sites for different space weather events: magnetic storm and Pi3 pulsations. We compare the spectral content of geomagnetic, telluric, and GIC variations. This comparison shows that the commonly used as a measure of GIC disturbances time derivative of geomagnetic field dB/dt does not totally control them. The suppression of high-frequency component in the GIC spectrum as compared with dB/dt variations is determined by the frequency-dependent character of the crustal geoelectric response.

Keywords GIC · Magnetic storm · Telluric fields

1 Introduction

As advanced technologies are implemented more widely, they have become increasingly subject to failures and interruptions due to the influence of space weather. This natural tendency cannot be avoided, and these vulnerabilities may increase as

O. Kozyreva (✉) · E. Sokolova
Institute of Physics of the Earth, Moscow, Russia
e-mail: kozyreva@ifz.ru

V. Pilipenko
Geophysical Center, Moscow, Russia

Ya. Sakharov
Polar Geophysical Institute, Apatity, Russia

D. Epishkin
Nord-West Limited, Moscow, Russia

these systems continue to evolve. Magnetic storms and substorms have potential to cause serious failures of space and ground technological systems. One of the most significant factors of space weather for terrestrial technological systems is electric geomagnetically induced current (GIC) in technological conductor systems related to abrupt changes of the geomagnetic field dB/dt [4, 6]. GICs associated with great magnetic disturbances were found to be dangerous for technological systems, causing malfunctioning of railway equipment [2, 10], disruption of ground and transatlantic communication cables, and reduction of the lifetime of pipelines.

Besides that, there are numerous examples of the noticeable consequences of space weather for extended high-voltage power grids. GICs caused saturation, growth of harmonics, overheating and even damage of high-voltage transformers. The most intense currents (over hundreds of Amperes) have been measured in the neutral leads of transformers at auroral latitudes during magnetic storms and substorms [7]. There is no general rule of how strong GIC should be to become harmful, since there are many types of transformers with different sensitivity to GIC. For some power transformers only a few Amperes are needed to shift the transformer operation from a linear regime [11].

Ongoing expansion of high-voltage power networks, growth of linkage between them, increase of load, and transition to low-resistive transmission lines with higher voltage lead to an increased probability of accidents during space weather events. Moreover, catastrophic failures are not necessarily required in order to have a detectable economic impact because of the way that wholesale electricity markets operate. The most likely consequence of a major geomagnetic storm, if not mitigated, is a widespread system voltage collapse [8]. Therefore, even if power infrastructure hardware is not lost during severe space weather events, GICs in regional power grids can still have broad flow-on effects throughout the global economy [3].

The highest risk of GIC may be related not directly to large-scale auroral currents, but too much weaker, but fast, small-scale processes. Though the power of such processes is many orders of magnitude lower than the power of magnetospheric storms and substorms, their rapidly varying electromagnetic fields can induce a significant GIC [1, 12]. So, information about GIC may be important from a fundamental scientific viewpoint, revealing a fine structure of fast geomagnetic variations during storms and substorms.

The difference of the electric field potential in the surface layers of the crust is responsible for GICs in grounded electric power systems. However, direct information on geoelectric fields is not easily available. While the geomagnetic field variations are monitored by world-wide array of magnetometers (>300), regular long-term observations of telluric electric fields are not so common yet. Moreover, information on GICs is property of commercial companies and is not available for the world scientific community for in-depth analysis.

Commonly, it was assumed that intensity of GIC J is proportional to time derivative of the geomagnetic field, $J \sim dB/dt$ [12]. However, this relationship is valid for a closed circuit with a conductive resistance in a free space only. In realistic situations, a contour where GICs flow, is formed by transmission lines, ground contacts, terminating transformers, and ground. The electric parameters of those elements—resistivity

and induction, as well as their dependence on frequency, are known very approximately. The actual relationship between the spectral contents of magnetic variations ΔB, telluric electric field E, and GIC J is a question which our paper tries to answer.

2 Geomagnetic, Magnetotelluric and GIC Data

The system to monitor the impact of GIC on electric power transmission lines has been deployed at Kola Peninsula and Karelia by the Polar Geophysical Institute (Apatity) and Center for Physical and Technical Problems of North's Energetic (Apatity) [9]. The system consists of 4 stations at a 330 kV power line and a station at a 110 kV power line (see map in Fig. 1). Each station records with a 1 min sampling rate a quasi-DC current in dead-grounded neutral of the autotransformer in the power line.
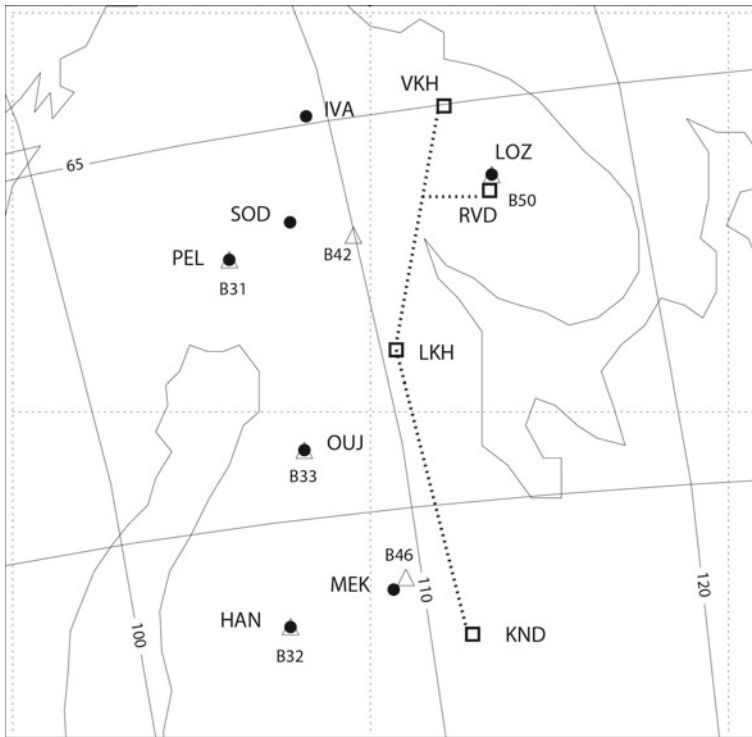

Fig. 1 Map showing magnetic IMAGE stations (black dots), selected BEAR deep sounding sites (empty triangles), and GIC recording stations (empty squares). Dotted lines denote power transmission lines. Thin solid lines denote the geomagnetic coordinates

To characterize the general geomagnetic disturbance level in the region under study we use the regional electrojet index EI (http://space.fmi.fi/image/www/). Local geomagnetic variations are monitored using 10 s data from the IMAGE magnetometers located in the vicinity of GIC recording stations (Fig. 1).

The telluric electric fields were calculated, using the available impedance data. The spatial distribution of crustal conductivity in the Eastern Fennoscandian Shield is very inhomogeneous. The comparison between impedances of several characteristic sites is given in Fig. 2. At period $T = 90.5$ s the largest $|Z|$ is near PEL (B31), ~10 mV/km nT. The ~4 times lower $|Z|$ is near OUJ (B33), ~2.4 mV/km nT. Rather high $|Z| \sim 7.2$ mV/km nT is near LOZ (B50). Thus, for the same magnetic disturbance, the telluric E-field contrast between different points may be as high as several times. Therefore, for precise estimates even a small deviation between the location of geomagnetic observatory, MTS sites, and GIC stations might be important. Essential magnitudes of the off-diagonal elements of the tensor Z (Fig. 2) indicate that the geoelectric properties of the crust are strongly anisotropic.

Constrained by data availability we used the following groups of the IMAGE, BEAR, and GIC stations: closely located LOZ—B50—RVD, and the magnetic and GIC stations at the same geomagnetic latitudes IVA—VKH.

2.1 Telluric Field Calculations E

The telluric E-field has been synthesized according to the following scheme. The algorithm of telluric E(t) field synthesis from geomagnetic field variations $\Delta B(t) =$
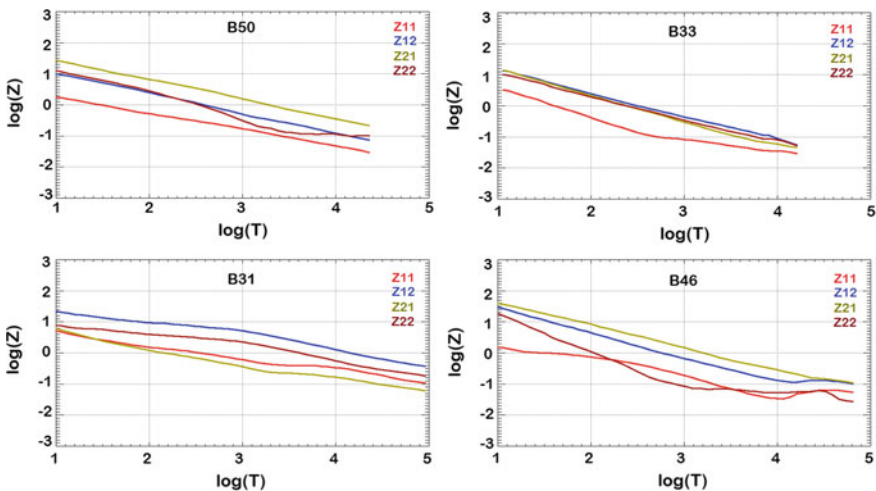

Fig. 2 The dependence of amplitudes of impedance tensor elements $Z_{i,j}$ (where x is Northward, y is Eastward) on period T at several sites of BEAR array

$\{X(t), Y(t)\}$ uses the standard frequency domain relationship between electric $\boldsymbol{E}(f)$ and magnetic $\boldsymbol{B}(f)$ fields via the complex impedance tsor $\boldsymbol{Z}(f)$, as follows

$$\begin{pmatrix} E_x(f) \\ E_y(f) \end{pmatrix} = \mu_o^{-1} \begin{pmatrix} Z_{xx} & Z_{xy} \\ Z_{yx} & Z_{yy} \end{pmatrix} \begin{pmatrix} X(f) \\ Y(f) \end{pmatrix}. \tag{1}$$

The elements of the impedance tensor in the range of periods T from 8 s to 55,000 s are known from the results of the BEAR experiment in 1998 [5]. The Fourier transform is applied to detrended magnetic records in a running time window to produce a set of spectral estimates of $\Delta \boldsymbol{B}(f)$ and from (1) the corresponding spectral estimates of telluric field $\boldsymbol{E}(f)$. The inverse Fourier transform performed for each running window. Thus, for a specific moment of time we have several electric field estimates, which are averaged to get final synthetic electric field time series E(t). The program was successfully tested on the synthetic magnetic and electric fields of COMDAT project. Further, we use the synthesized telluric fields together with geomagnetic data for several space weather events to search for factor responsible for the GIC excitation.

3 Magnetic Storm 2012, Nov. 12–14

This strong magnetic storm (|SYM-H| > 100 nT) was caused by fast solar wind streams. During the period Nov. 14, 00–04 UT a series of short-term auroral intensifications occurred as evident from the local electrojet intensity (EI) index (up to ~1500 nT) (Fig. 3). Two irregular substorm-related intensifications reaching maximum at IVA-LOZ occurred at ~01 UT and ~0220 UT. At a lower latitude (OUJ) maximum of magnetic disturbance was observed at ~0150 UT. The spike of EI-index at ~0330 UT is due to a more distant activation.

During this period intense fluctuations of GIC were recorded in all elements of the power transmission line. The most intense GICs, with peak-to-peak amplitudes up to ~60 A, were recorded at VKH. We compare GIC intensity J at VKH, magnetic field variations X and time derivative dX/dt at IVA, and telluric fields Ex, Ey at IVA/B50 (synthesized via impedance at B50 site) (Fig. 4). The bursts of J occur in coherent way with intensifications of dX/dt (up to ~100 nT/s) and E-field (up to several V/km) throughout all stations.

Even visual comparison shows that fluctuations of dX/dt are more high-frequency as compared with E and J. The spectral analysis confirms this conjecture (Fig. 5). To compare in detail the spectral features of geomagnetic, telluric, and GIC variations we have normalized their spectra. The spectral components at frequencies ~4 and ~6 MHz are highlighted in the spectrum of $J(f)$ and X'(f) ($X' = $ dX/dt). These components are due to the contribution from the fast fluctuations in the Pi3 range embedded in the auroral electrojet intensification. But, in general, the spectrum of $X'(f)$ strongly deviates from the spectra of $J(f)$ at higher frequencies (>5 MHz) and
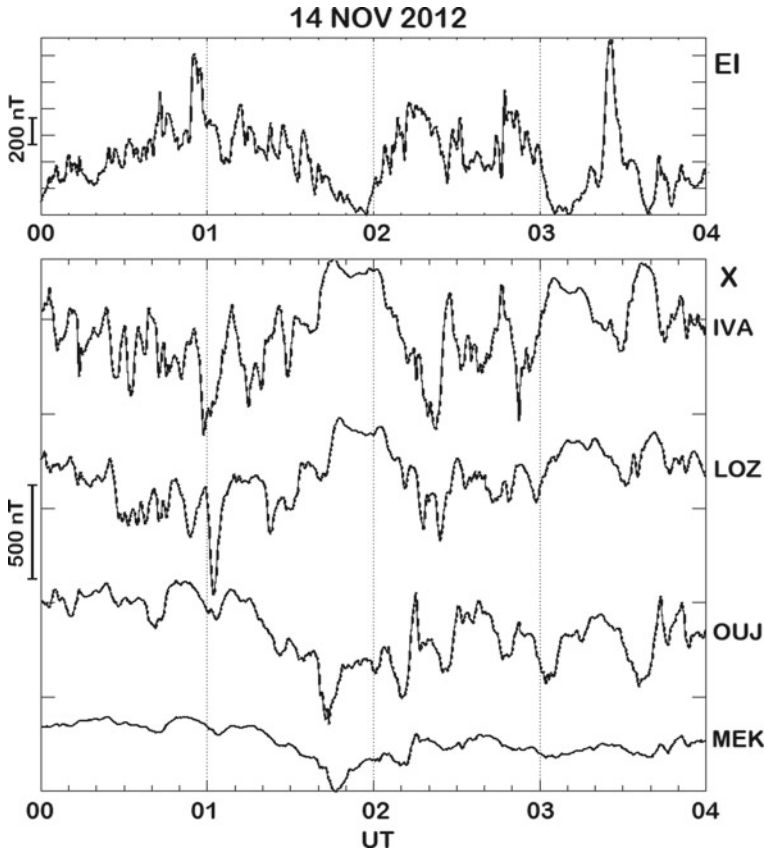
Fig. 3 Variations of the geomagnetic field during magnetic storm at 2012, Nov. 14, 00–04 UT: regional EI-index, *X*-component of magnetic disturbance (North) at the IMAGE stations IVA, LOZ, OUL, and MEK

is much closer to $Ex(f)$. Thus, the ground geoelectric properties play a role of a low-pass filter for geomagnetic variability dB/dt.

4 Pi3 Pulsations During the Magnetic Storm on 2013, June 29

The magnetic storm on June 27–29 started with the interplanetary shock arrival on June 27, ~15 UT. The interplanetary magnetic field (IMF) *Bz* since June 28, 08 UT gradually turned southward ($Bz < 0$) and kept steady at the level about −10 nT till June 29, 12 UT. Such IMF orientation produced driving of the magnetosphere into
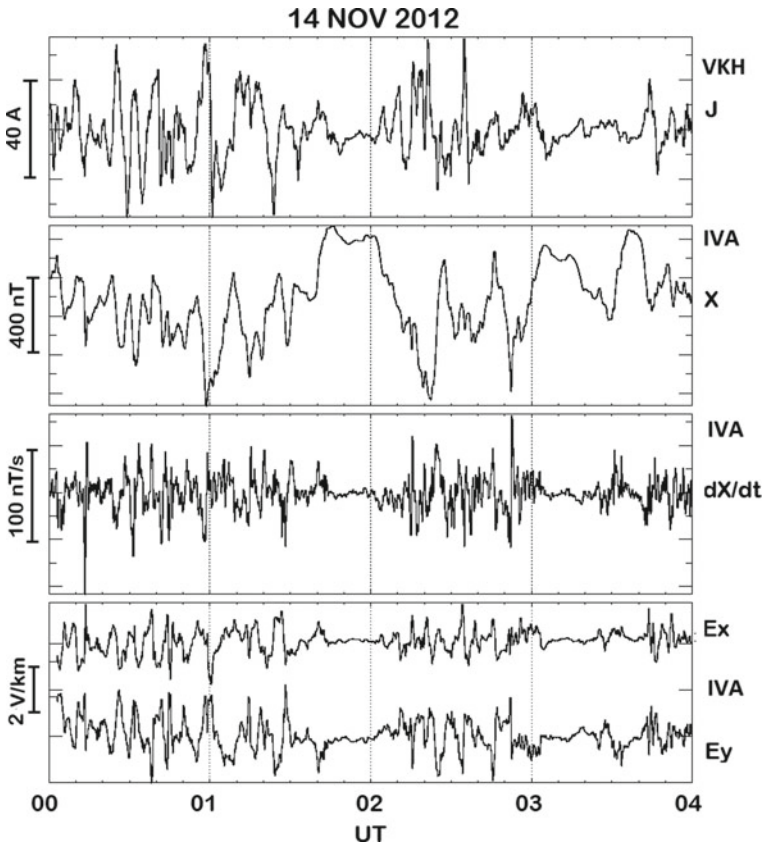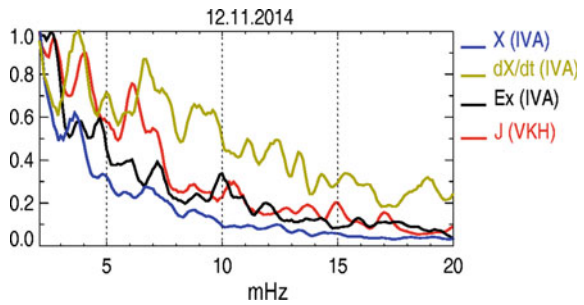
Fig. 4 GIC intensity *J* (A) at VKH, magnetic field variations *X* (nT) and time derivative *dX/dt* (nT/s) at IVA, and telluric fields *Ex* (V/km) and *Ey* (V/km) from IVA/B50

Fig. 5 Normalized spectra for the period 2012, Nov. 14, 01–03 UT: *J*(f) at VKH, *X*(*f*), *X′*(*f*), and *Ex*(*f*) at IVA

the magnetic storm with maximum |*Dst*| ~ 120 nT. During the storm's growth phase the EI-index shows gradual irregular growth (Fig. 6).

During the period of maximal magnetic disturbance, 00–04 UT, intense irregular variations with peak-to-peak amplitudes up to ~600 nT are superposed on the magnetic bay (Fig. 6). The time scale of these quasi-periodic oscillations (which may be classified as Pi3 pulsations) vary from ~20 min at lower latitudes up to ~10 min at higher latitudes. Most intense variations are observed at OUJ. Subsequent paragraphs, however, are indented.

During this storm extremely high values of GIC (peak-to-peak variations up to ~200 A) were recorded at station VKH on June 29, from 01 to 03 UT, at other stations GICs were weaker. Each Pi3 impulse was accompanied by a localized burst of GIC, magnetic field variability, and telluric current.
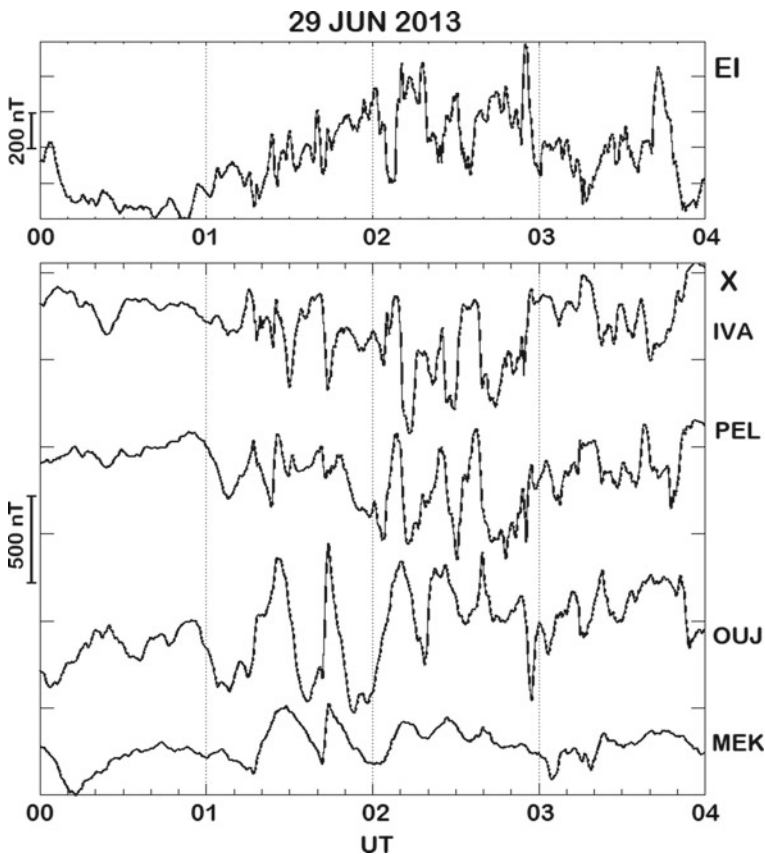

Fig. 6 Geomagnetic activity on 2013, June 29, 00–04 UT: EI-index, *X*-component of magnetic field variations at IMAGE stations LOZ, PEL, OUL, MEK
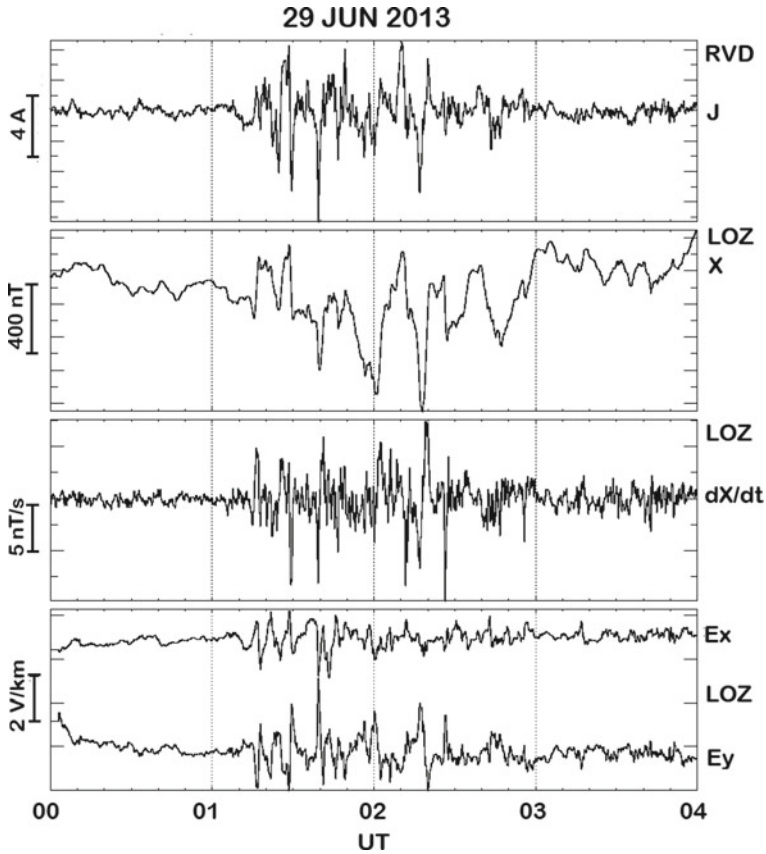
Fig. 7 Comparison of *J* at RVD with magnetic disturbances *X* and time derivatives of magnetic field d*X*/dt at near-by station LOZ, and *E*-field at LOZ/B50 during the Pi3 event on June 29, 20

The telluric field demonstrates irregular variations with different amplitudes at different locations (not shown). For example, the most intense E-field variations (>15 V/km) are observed at PEL, though at OUJ and PEL amplitudes of magnetic variations are nearly the same. This asymmetry is most probably caused by the ~2.5 times higher magnitude of crustal impedance at PEL as compared with that at OUJ.

For a detailed comparison of spectral features of GIC and terrestrial electromagnetic field we use observational data from two neighboring stations RVD and LOZ. Visual examination of *J* at RVD together with *X* and d*X*/dt at LOZ, and *E*-field at LOZ/B50 (Fig. 7) shows that for the interval under analysis the time derivative d*X*/dt correlates with variations of GIC not much better than just magnetic variation *X* does. This fact is confirmed by the spectral analysis (Fig. 8). Normalized overlaid spectra of all timeseries have a decaying character, with some enhancements at ~4 and ~7 MHz, provided by contributions from transient Pi3 impulses embedded in the

Fig. 8 Normalized spectra for the period 2013, June 29, 01-03 UT of J at RVD, X and dX/dt at LOZ, and Ex at LOZ
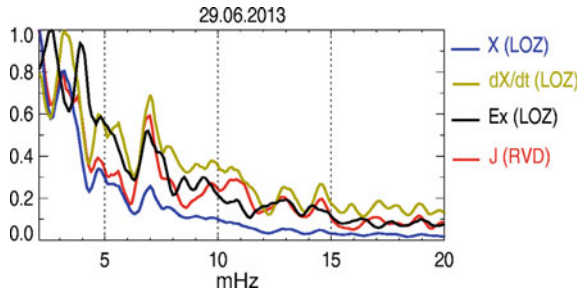
magnetic bay. The spectrum $X'(f)$ at higher frequencies is larger than the spectrum $J(f)$. At the same time, the spectrum $Ex(f)$ is closer to the spectrum $J(f)$ at $f > 7$ MHz.

5 Discussion and Conclusion

Examination of several space weather events has shown that ground geoelectric properties play a role of a low-pass filter for geomagnetic variability *dB/dt*. The high frequency component of the spectra of "response"—telluric fields and GICs, is suppressed as compared with the spectrum of a driving *dX/dt* fluctuations. In the Fennoscandia region contrast between the telluric E-field in different points may be as high as ~3–4 times for the same amplitude of magnetic disturbance. Therefore, even a small deviation between the location of a geomagnetic observatory, MTS site, and GIC station might be important for precise studies. Spectral analysis revealed enhancements at typical Pi3 frequencies (~2–3 and ~ 5–7 MHz) of GIC due to contribution of sporadic impulses embedded in the magnetic storm evolution.

References

1. Belakhovsky, V.B., Pilipenko, V.A., Sakharov, Ya.A., Selivanov V. N.: Characteristics of the variability of a geomagnetic field for studying the impact of the magnetic storms and substorms on electrical energy systems. Izv. Phys. Solid Earth, **54**(1), 52–65 (2018)
2. Eroshenko, E.A., Belov, A.V., Boteler, D., Gaidash, S.P., Lobkov, S.L., Pirjola, R., Trichtchenko, L.: Effects of strong geomagnetic storms on Northern railways in Russia. Adv. Space Res. **46**, 1102–1110 (2010)

3. Forbes, K.F., St. Cyr, O.C.: Space weather and the electricity market: An initial assessment. Space Weather **2**, S10003 (2004). https://doi.org/10.1029/2003SW000005
4. Knipp, D.J.: Synthesis of geomagnetically induced currents: commentary and research. Space Weather **13**, 727–729 (2015)
5. Korja, T., et al.: Crustal conductivity in Fennoscandia—a compilation of a database on crustal conductance in the Fennoscandian Shield. Earth Planets Space **54**, 535–558 (2002)
6. Lanzerotti, L.J.: Space weather effects on technologies. Space Weather Geophys. Monogr. Ser. AGU. **125**, 11–22 (2001)
7. Pirjola, R. Kauristie, K., Lappalainen, H., Viljanen, A., Pulkkinen, A.: Space weather risk. Space Weather **3**, S02A02 (2005). https://doi.org/10.1029/2004SW000112
8. Pulkkinen, A., et al.: Geomagnetically induced currents: science, engineering and applications readiness. Space Weather **15**, 828–856 (2017)
9. Sakharov, Ya.A., et al.: Registration of GIC in power systems of the Kola Peninsula. In: Proceedings of 7-th International symposium on Electromagnetic Compatibility and Electromagnetic Ecology, St-Petersburg, pp. 291–293 (2007)
10. Sakharov, Ya.A., et al.: Geomagnetic disturbances and railway automatic failures. In: Proceedings of 8th International Symposium on Electromagnetic Compatibility, St-Petersburg, pp. 235–236 (2009)
11. Vakhnina, V.V., Kuvshinov, A.A., Shapovalov, V.A., Chernenko, A.N., Kretov, D.A.: The development of models for assessment of the geomagnetically induced currents impact on electric power grids during geomagnetic storms. Adv. Electr. Comput. Eng. **15**, 49–54 (2015)
12. Viljanen, A., Nevanlinna H., Pajunpää, K., Pulkkinen A.: Time derivative of the geomagnetic field as an activity indicator. Ann. Geophys. **19**, 1107–1118 (2001)